PCCP

PAPER

View Article Online
View Journal | View Issue

Cite this: *Phys. Chem. Chem. Phys.*, 2026, **28**, 7344

Identification of the roaming mechanism and the formation of H_3^+ in core ionised cyclopropane

Ville Lindblom, *[a] Smita Ganguly,[b] Noelle Walsh,[c] Mathieu Gisselbrecht [a] and Stacey L. Sorensen [a]

Received 17th December 2025,
Accepted 24th February 2026

DOI: 10.1039/d5cp04926a

rsc.li/pccp

Spectroscopic validation of the roaming process in molecular dissociation was first reported for formaldehyde, but today roaming is acknowledged to be a nearly ubiquitous dissociation pathway. The process has been described as a frustrated dissociation process, and as such, direct detection of the roaming process is challenging. In the present study the cyclopropane dication is the starting point for a roaming process that results in the production of H_3^+. In our experiment, we measure the complete momenta of all charged fragments and unravel the kinematics for relevant fragmentation processes. We present a comprehensive study of the process comparing alternative pathways for dissociation and their kinematics in association to the roaming process. In this study, inner-shell electron ionisation leads to dication states, these final electronic states are fundamentally identical to ones reached *via* direct double ionisation.

Introduction

Understanding the interaction between molecules and light is of fundamental importance as it plays a key role in a wide variety of systems in biology, chemistry, and physics, of relevance for key processes in a broad set of applications spanning from biomolecules to plasma physics. Photoionisation with ionising radiation rapidly changes the electronic configuration of the molecule generally driving a slower evolution of molecular geometry although dissociation is known to take place in core-excited states.[1,2] A core-ionised or excited electronic state is short lived, but the system may evolve before electronic decay, and both isomerisation and bond extension in the neutral core-excited molecule are common.[3–5] Electronic decay *via* auto-ionisation populates electronic states in the single-, double- and triple ionisation continuum, *i.e.* in the inner-valence region of the spectrum. Consequently, higher charged ions will dissociate, typically through bond elongation until the bond breaks or by overcoming a potential barrier which includes a higher energy transition state. However in recent years a new dissociation pathway after molecule and light interaction has been invoked, namely "roaming".

The "roaming process" as a molecular dissociation pathway was first discovered in formaldehyde, but it was quickly found in other small neutral molecules.[6–10] Just a few years after the discovery in formaldehyde the roaming dissociation pathway was found in dications as well, showing that roaming indeed is a ubiquitous dissociation mechanic in small molecules and ions.[11,12] Since then it has been identified as an important mechanism in several other molecules and the mechanics have become more and more understood, although some questions still remain.[13–23] The key characteristic of the process in a dication is that a neutral moiety is emitted from the parent dication in the first step. The neutral moiety is captured by a shallow potential energy well and migrates around the parent. Eventually, the neutral moiety abstracts a charged fragment from the parent, resulting in a charge separation between two weakly-bound fragments. The system breaks apart due to Coulomb repulsion between the two charged fragments. In the case of roaming with a neutral parent, the steps occur in a similar manner but with different kinematics and charge dynamics; The neutral case is thoroughly described by Bowman *et al.*[13] One commonly observed product of the roaming process is the H_3^+ ion, created from the roaming of a H_2 or possibly a hydrogen atom.[11,12,16,21,24]

The trihydrogen cation (H_3^+) is one of the most abundant ions in the universe and is found primarily in the interstellar medium.[25] H_3^+ plays an important role in both atmospheric and interstellar chemistry due to its high reactivity. This property highlights the role of H_3^+ in facilitating formation of larger hydrocarbons and water, making it important to understand the origin of the trihydrogen ion in space.[21]

In an earlier study that focussed on the inner-valence region and thresholds for specific fragmentation channels we found

[a] *Department of Physics, Lund University, Box 118, Lund, 221 00, Sweden. E-mail: ville.lindblom@fysik.lu.se*
[b] *J. R. Macdonald Laboratory, Department of Physics, Kansas State University, Manhattan, KS 66506, USA*
[c] *MAX IV Laboratory, Lund University, Box 118, Lund, 221 00, Sweden*

that cyclopropane exhibits a H_3^+ peak in the mass spectra following photoionisation with photon energies above 31.25 eV.[26] In that paper a novel vibrationally-active dissociation process was invoked to explain the formation of H_3^+ in which the carbon 'triangle' was intact. Kwon *et al.*[27] compared the time scale for production of H_3^+ from cyclopropane and from propene using time-resolved mass spectrometry. The similarity between the measured timescales for the process in the cyclic and linear isomers provided evidence for ring breaking in cyclopropane, and the roaming process was suggested as the mechanism behind H_3^+ formation following double ionisation.

In this study we utilise synchrotron radiation to investigate dissociation pathways in core-ionised cyclopropane. We take a detailed look at the creation of H_3^+ from the cyclopropane dication, including the role of roaming. We can directly observe evidence for this roaming process by measuring the full momenta of all fragmentation products. Specifically, we show that the roaming revolves around the neutral moiety H_2 moving around the $C_3H_4^{2+}$ dication. We discover that this dication can dissociate in several different ways before the formation of H_3^+ can occur. The $C_3H_3^+/H^+/H_2$ fragmentation pathway show two possibilities, one where roaming occurs and one where a concerted dissociation of the three fragments occurs. These two possibilities are disentangled, and the roaming pathway is shown to fail the abstraction of a proton only when the accessible internal energy is too low to form the H_2–H^+ bond. When that energy is exceeded the $H_3^+/C_3H_3^+$ pair is produced instead.

Experimental method

The experiment was conducted at the Flexible Photon-Electron Spectroscopy (FlexPES) beamline[28] at the 1.5 GeV storage ring at MAX IV in Lund, Sweden. The beamline provides horizontally polarised light which interacts with a cold supersonic jet of cyclopropane. The cyclopropane liquid (Apollo Scientific, 99% purity) vaporised at room temperature without any additional heating. The jet was produced by two skimmers both with 1 mm diameter with a stagnation pressure of 1040 mbar with the pressure in the spectrometer chamber at $4.10 \cdot 10^{-8}$ mbar. The ICE (Ions in Coincidence with Electrons)[29] Reaction Microscope end station was used in a lens mode configuration using a relatively high applied electrostatic field (110 V cm^{-1}) at the interaction focus. The electric field serves to guide the charged particles (electrons and ions) produced in photoionisation process towards dedicated time- and position-sensitive detectors. For the fields used in this experiment the electron detector captures all photoelectrons up to an energy of 15 eV while the ion detector captures all ions up to 10 eV kinetic energy. The coincidence events are the result of the coincident detection of at least one electron and one ion, but may include up to five positively charged ions. Since we measure the 2D position (x and y) as well as the time of flight (TOF), the full 3D momenta of all particles can be extracted. All measurements were taken at 299.1 eV photon energy, about 9 eV above the C1s ionisation threshold.[30] The TOF start is given by a bunch marker provided from the storage ring. The coincidence measurements were taken with an ion detection rate of 1 kHz to minimise false coincident detections.

Results and discussion

In Fig. 1(a) the mass spectrum measured after inner-shell photoionization at 299.1 eV is shown. The parent ion ($C_3H_6^+$) is barely visible in the spectrum, but fragments based on C_3 with peaks for C_3^+ to $C_3H_3^+$ are clearly visible as well as features arising from C2- and C-based fragments, which are broadened due to kinetic energy. We also observe a distinct peak corresponding to H_3^+, and narrow dication peaks around 20 Da. The ion–ion correlation map in Fig. 1(b) shows that the H_3^+ ion is formed mainly in the ion–ion fragment pair $H_3^+/C_3H_3^+$ (this pathway has been attributed to the roaming process[27]).

There are many different fragmentation pathways available in cyclopropane; these can be grouped as follows: the $H_i^+/C_3H_j^+$ group in Fig. 1(b) requiring dissociation of a C–H bond and $CH_n^+/C_2H_m^+$ in Fig. 1(c) requiring dissociation of two C–C bonds. There are a few anomalous features visible in the ion–ion correlation maps. In particular, there are several instances of correlation maps with a total mass exceeding 42, *e.g.* the $C_2H_4^+/CH_3^+$ pair. The mass of this pair is one amu greater than cyclopropane molecules but based on its intensity we attribute this anomaly to be due to the relative abundance of naturally occurring isotopes of carbon. The relative yield of these pathways (relative to the measured intensity for mass 42 amu) corresponds well to the known natural carbon-13. Secondly, some weak lines in the PEPIPICO plot seems to be 'shadows' of the main fragmentation channels separated by about 10 ns, for example below $H_3^+/C_3H_3^+$. These arise as a result of electrons ejected from the spectrometer mesh in connection with an ion. Because of a field free region between the mesh and the MCP, such an electron can hit the MCP and register as an ion hit. Simulated time for this to occur is in agreement with the 10 ns separation. Due to the nature of these hits being registered as an extra ion with a set time shift in a coincidence measurement, they can be filtered out by hit selection. These features have thus been neglected in the analysis.

In the ion–ion correlation map of the measurement in Fig. 1(b) we see a ''tail'' extending from the $C_3H_3^+/H^+$ fragment pair. This suggests a ''metastable state'' of the dication. Typically, the dication dissociates within the interaction region, and thus the TOF through the drift region would be dependent on the mass (and charge) of the fragment. In the case of a dication in a metastable state, the doubly charged ion breaks apart inside the drift region, creating a long distribution in TOF that is visible in the correlation map extending from the coincidence islands. Meaning that the TOF is no longer only dependent on the mass and charge, but also on the lifetime of the dication. Using the method described by Field *et al.*[31] we can calculate a lifetime for the dication and it is found to be $\tau = 326 \pm 26$ ns. Clearly, the

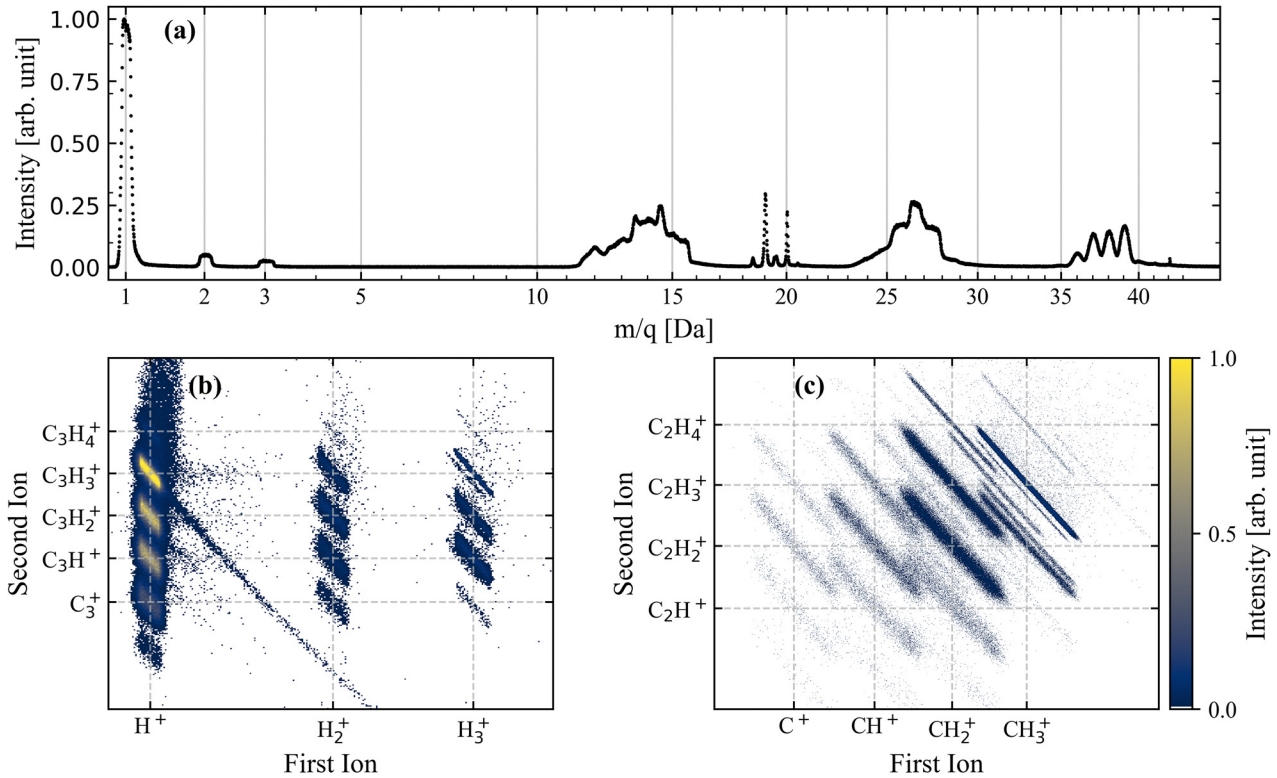

Fig. 1 (a) Mass spectrum measured at 299.1 eV photon energy from cyclopropane. A weak feature from the $C_3H_6^+$ ion is visible at 42 Da. Five groups of peaks are visible. The first group (1–3 Da) is from hydrogen-based ions (H^+, H_2^+ and H_3^+). The next group (12–15 Da) arises from ions consisting of a single carbon and up to three hydrogens. The group at 24–29 Da contains two carbons and up to five hydrogens while the last group at 36–42 Da is based on three carbons. The sharp peaks at 19.5–20.5 Da are dication peaks. Ion–ion correlation maps of two regions of interest are also displayed. The channels (b) $C_3H_n^+/H_m^+$ arise after only C–H bond dissociation and (c) $C_2H_x^+/CH_y^+$ require two C–C and possible C–H bond dissociations. Narrow correlation lines indicate complete fragmentation while when mass is lost to neutral particles the distributions are broadened.

metastable tail contains only a small percentage of the main fragmentation pair (7.48 ± 0.94%).

For a roaming process to take place in this system, both a neutral moiety and an associated dication are needed. As mentioned previously the literature has shown that neutral H_2 is pivotal in H_3^+ formation. In Fig. 1(a) two dications are most prevalent, $C_3H_4^{2+}$ and $C_3H_2^{2+}$. Kwon *et al.*[27] noted that dication species which emerge from cyclopropane primarily contain an even number of hydrogen atoms, thus assuming that emission of neutral H_2 from the dication is favoured. We conclude that roaming involves neutral H_2 moving around the doubly charged $C_3H_4^{2+}$.

Analysing the roaming of H_2 requires imaging fragmentation during the process. In our measurement we determine the complete momenta of all fragments, including any neutral species produced in the process. Knowing the momenta of the measured particles we can retrieve the momentum of the undetected particle through conservation of momentum. This is also formally true for more than one undetected particle, although for multiple neutral particles the sum is detected rather than the individual momentum vectors. For the case of complete fragmentation, roaming must occur around the dication $C_3H_4^{2+}$. Thus, by measuring the fragments originating from $C_3H_4^{2+}$ we obtain the momenta of all particles including the neutral H_2 moiety. This dication may dissociate *via* three different pathways that preclude formation of H_3^+. A single C–H bond could break producing the $H^+/C_3H_3^+$ pair, two C–H bonds could break and a H–H bond form producing the $H_2^+/C_3H_2^+$, or lastly a C–C bond could break resulting in either $CH^+/C_2H_3^+$ or $CH_2^+/C_2H_2^+$. An additional possibility could be charge transfer from the neutral moiety to the dication resulting in the $H_2^+/C_3H_4^+$ pair. The latter pathway is not considered further since the fragment pair is missing in the correlation map of Fig. 1(b).

The momentum analysis of these fragmentation pathways provides information on how the dication dissociates. The Dalitz plot[4,32–34] and Newton diagram[35,36] are useful tools to study these dissociation processes and identify their dynamics. In Fig. 2(a)–(c) these figures and a histogram of the associated angles are shown for the $H^+/C_3H_3^+$ pair. The other channels ($H_2^+/C_3H_2^+$ and $CH_2^+/C_2H_2^+$) are displayed in SI Fig. S1(a)–(f). The Dalitz plots are constructed in phase space using the normalised coordinates $x = \left(\varepsilon_{P_3} - \varepsilon_{P_2}\right)/\sqrt{3}$ and $y = \varepsilon_{P_1} - \frac{1}{3}$, where $\varepsilon_i = |\mathbf{P}_i|^2 \Big/ \sum_n |\mathbf{P}_n|^2$ for all n ions with each ion i having the momentum $\boldsymbol{P}_i$. The Newton diagram shows the momentum vectors of the three fragments in the molecular frame. Due to momentum conservation, the three vectors are coplanar. One

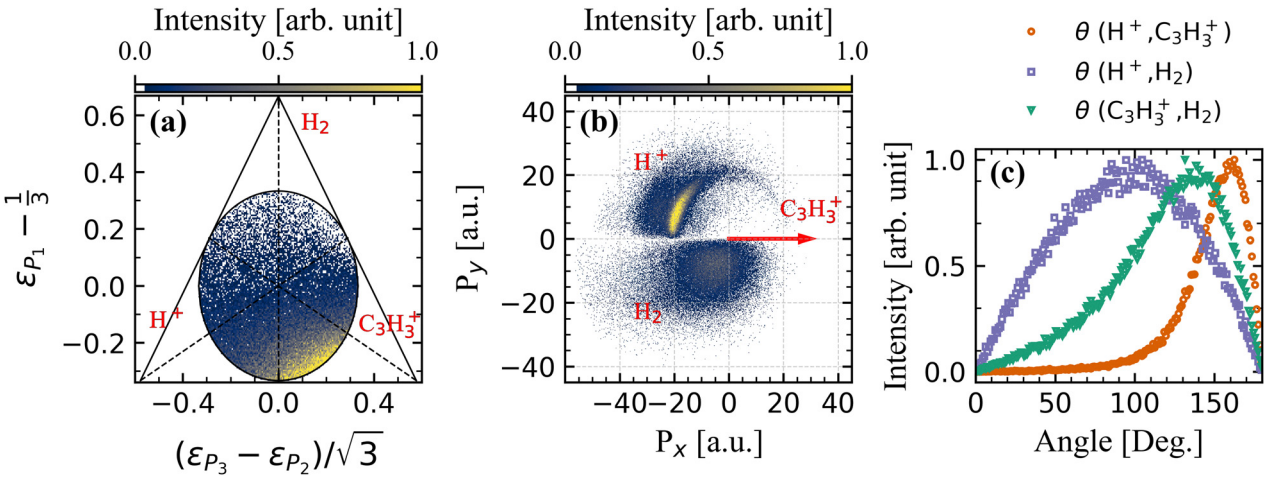

Fig. 2 The momentum vector distribution from the fragmentation channel $H_2/H^+/C_3H_3^+$. (a) Dalitz plot with ε_{P_1}, ε_{P_2} and ε_{P_3} representing H_2, H^+ and $C_3H_3^+$, respectively. (b) Newton diagram with the H_2 and H^+ momentum vectors mapped relative to $C_3H_3^+$. (c) Angular distribution between the three momentum vectors. The intensities for the angular distributions are normalised.

fragment (the heaviest) is chosen as the reference axis, while the other two fragment vectors are calculated relative to that axis. Therefore, one of the fragments will solely be mapped onto the upper half ($P_y > 0$) and the other on the lower half ($P_y < 0$).

The momentum distribution for the fragmentation channel $H_2/H^+/C_3H_3^+$ in Fig. 2 shows a complex dissociation pattern. The Dalitz plot in Fig. 2(a) does not show any clear indication of the dissociation mechanism, while in contrast, SI Fig. S1(a) and (d) show much clearer indication of concerted and asynchronous concerted dissociation, respectively. The channels shown in the supplementary information exhibit no indication of the roaming mechanism. Both Fig. 2(b) and (c) show a strong resemblance to the momentum distributions found in acetonitrile, which Mishra *et al.*[16] concluded to be a signature of roaming. The neutral H_2 exhibit a broad momentum distribution which is consistent with what would be expected for a neutral fragment. Furthermore, the proton momentum shows part of a half circle, indicating that its angle is dependent on the fragment on the opposite side, H_2. This pattern is consistent with what is expected in roaming. In Fig. 2(c) the two charged fragments dissociate at an angle of $\sim 160^\circ$. For a regular two body dissociation a 180° angle is expected, as seen in SI Fig. S1(c). The smaller angle suggests influence from a third body at the time of dissociation. The two other angles in Fig. 2(c) display both a broader distributions and more shallow angles, in particular the angle between H^+ and H_2 which here show an almost perfect random distribution. However, Fig. 2(b) indicates that there are two different distributions for the proton, one of higher kinetic energy and one of lower kinetic energy, the latter exhibiting stronger angular correlation.

Two different momentum distributions indicate two separate pathways. Fig. 3 shows the kinetic energy release (KER) of the two charged fragments, the energy released in the Coulomb repulsion, as a function of the total KER including the energy from the neutral H_2. Two regions emerge: the purple dashed

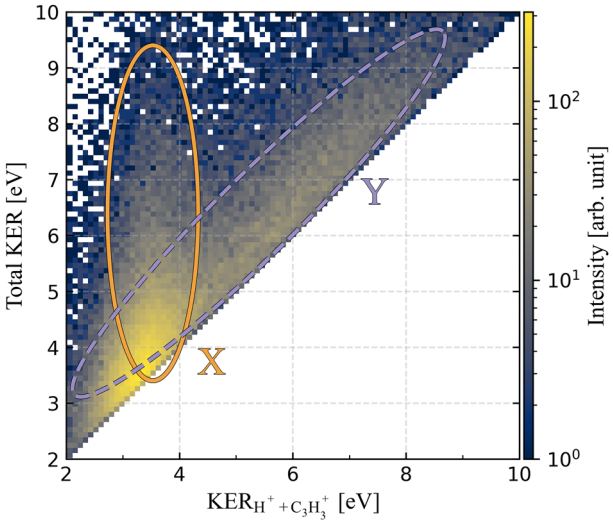

Fig. 3 The kinetic energy release diagram for the fragmentation channel $H_2/H^+/C_3H_3^+$. The *x*-axis display the energy released from the Coulomb explosion or the bond break, while the *y*-axis is the total kinetic energy release or the sum of kinetic energy from all fragments. Two regions of interest are marked: region *X* marked with a solid orange line and region *Y* marked with a dashed purple line.

region shows a pathway (*Y*) in which all the energy is released within the Coulomb repulsion from the two charges, leaving H_2 with almost no kinetic energy. The second solid orange region shows a pathway (*X*) where the Coulomb repulsion energy remains the same (~ 3.36 eV) while the total KER rises. All excess energy is deposited into kinetic energy of the H_2. The two regions overlap a considerable amount from ~ 3.36 eV (where pathway *X* emerges) to 6 eV. The *X* channel starts to deplete around 7.5 eV total KER while the *Y* channel only starts to deplete at around 9.5 eV. After 10 eV only noise remains for these channels as can be better seen in the supplementary information.

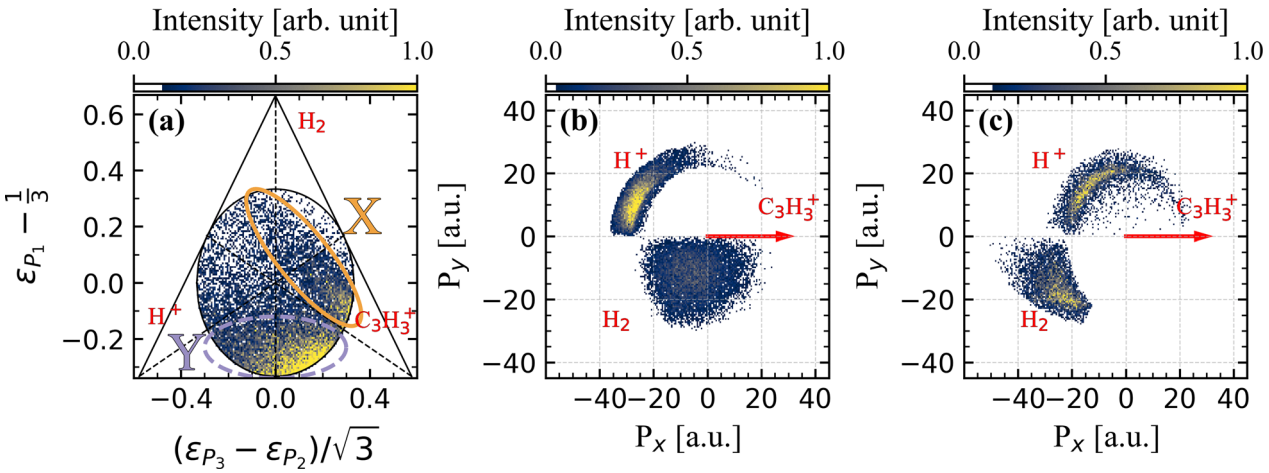

Fig. 4 Dalitz plot (a) for the fragmentation channel $H_2/H^+/C_3H_3^+$, filtered by $KER_{Total} > 6$. The two visibly separate regions *X* and *Y* are marked by a solid orange line and a dashed purple line, respectively. Newton diagrams for the respective filtered pathways *Y* (b) and *X* (c) show the distribution of the momentum vectors. The heaviest ion $C_3H_3^+$ is aligned with the *x*-axis while the other two momentum vectors are calculated relative to it.

Fig. 4(a) shows the momentum correlation for the higher total KER events ($KER_{Total} > 6$ eV); the two different pathways are clearly discernable. The *Y* pathway is typical of an asynchronous concerted process, while the *X* pathway indicates a more sequential type of dissociation. However, the *X* pathway's dissociation is not unambiguous as lower H_2 energy is strongly preferred. The nature of the roaming pathway is somewhat sequential in nature up until the point of successful proton abstraction after which it becomes a two-body concerted breakup. As the channel in question is interrupted by the C–H bond break a more sequential type of dissociation for this interrupted roaming channel is expected.

The momentum distribution in combination with the KER reveal that pathway *Y* is an asynchronous concerted dissociation with no clear relation to roaming, while pathway *X* shows distinct roaming characteristics. Fig. 4(b) and (c) further emphasises this with Newton diagrams. Fig. 4(b) show that the vast majority of protons in pathway *Y* are emitted opposite $C_3H_3^+$ while H_2 show a random low energy contribution, as expected from a concerted reaction containing one neutral and two charged fragments. On the other hand, Fig. 4(c) show that the proton's emission angle is more varied, whilst the H_2 ion is concentrated opposite to the $C_3H_3^+$ ion and with far higher kinetic energy. In agreement with the data in Fig. 3, the proton energy is "fixed" and thus creates a half-circle. One could also consider that if the neutral H_2 would instead be two separate H particles we would see a similar pattern as for the H_2 in the *Y* channel, Fig. 4(b), but with a more concentrated and smaller distribution as two neutral would likely not emit in the same direction. This furthermore reveal that for the *X* channel the possibility of two H particles is even more unlikely due to the specific angular emission and high kinetic energy. Fig. 5 reveals that the KER between the charged fragments of pathway *X* matches very well with the KER of the successful roaming channel $H_3^+/C_3H_3^+$ suggesting a similar dissociation mechanism.

The major difference between the *X* channel (where roaming is interrupted) and the successful H_3^+ roaming channel is then the H_2. In the *X* channel the H_2 takes all the excess energy from the system, while in the H_3^+ channel the H_2 has bonded with

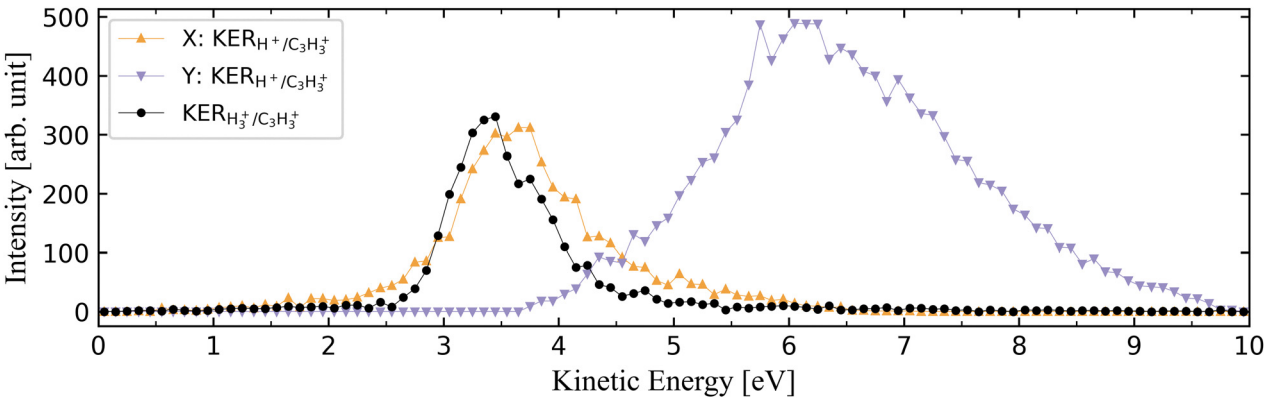

Fig. 5 The kinetic energy release of the charged fragments of the two channels *X* and *Y* ($KER_{total} > 6$) are compared with the kinetic energy released in the roaming channel were the H_3^+ ion is successfully formed.

the proton. This bond requires an energy of 4.35 eV to form.[37] The average KER of the charged fragments dissociation, E_{av} = 3.36 eV, plus the bond energy gives a total KER of approximately 7.70 eV. This is in the range of total KER were the *X* channel dies out in Fig. 3, indicating that when enough energy is delivered onto the roaming moiety it will start to successfully bond to the proton. Using this as a total average KER for the $H_3^+/C_3H_3^+$ pathway, and broadening it considering the KER resolution of the spectrometer (further details in the supplementary information), we can add those events to the KER diagram shown in Fig. 3 to create the sum shown in Fig. 6(a). The *X* channel is "filled in" at the higher kinetic energies, and the branching ratio, Fig. 6(b), indeed show a decrease in the *X* channel is replaced by an increase of the H_3^+ channel. Moreover, the summation of the *X* and $H_3^+/C_3H_3^+$ pathways has a constant 0.35 branching ratio in relation to pathway *Y*, indicating that the latter arises from the former at sufficient energy. Mishra *et al.*[16] suggest that if the CH bond in acetonitrile is strongly vibrationally excited, this energy is transferred to the H_2 in the form of kinetic energy. They did however conclude that the neutral moiety of the interrupted roaming channel had a low (<1 eV) kinetic energy, which is not the case for cyclopropane. We find that H_2 has a wide range of energies in the interrupted roaming channel *X*, all the way up to the binding energy needed to form the H_2–H^+ bond. At that energy H_3^+ formation takes over, providing clear evidence for H_3^+ formation through internal energy conversion between the vibrationally active CH and the roaming H_2. An interesting detail of the mechanistic picture in roaming as developed by Mishra *et al.* is a H_2 emission and rebinding cycle before the proton is successfully abstracted.[16] The *X* channel show no such dynamic but one could consider that the *Y* channel is a dissociation at the rebinding stage. This is merited by the fact that the dynamic of the *Y* channel is asynchronous concerted, in essence a concerted dissociation during a geometrical change. If this is the case one would expect the *Y* channel to exist in the exact same time scale as the *X* channel which is longer than most dissociative pathways. The data presented here cannot discern this time information but the experimental data provided by Mishra *et al.*, which is not separated into two channels, remains the same over the entire time window that they measure. This indicates that the mechanistic picture provided is valid and the *Y* channel is at least partly due to dissociation during the rebonding of the neutral H_2.

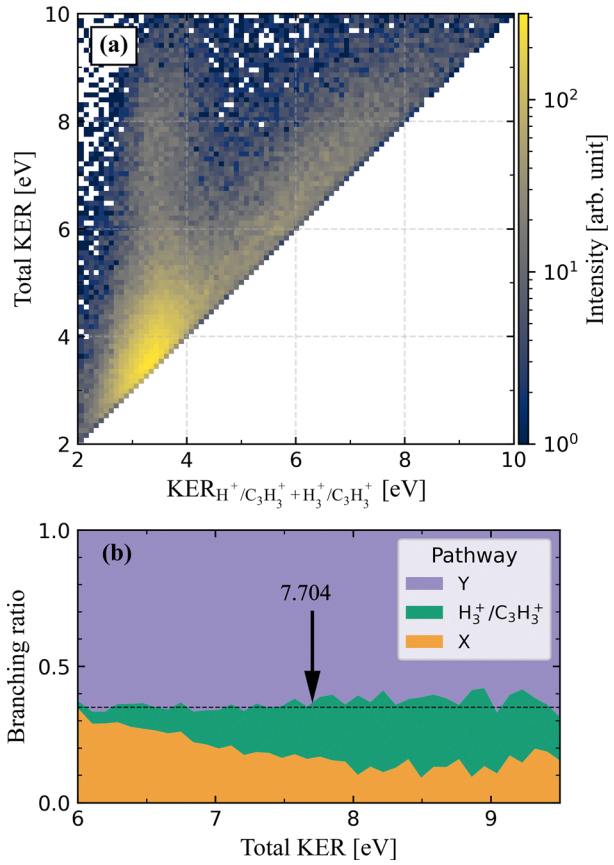

Fig. 6 (a) The kinetic energy release diagram for the summation of the fragmentation channels $H_2/H^+/C_3H_3^+$ and $H_3^+/C_3H_3^+$. The *x*-axis displays the energy released from the Coulomb explosion or the bond break, while the *y*-axis shows the total kinetic energy release. (b) The branching ratios of the three pathways, separated above 6 eV in total KER. A dashed line at 0.35 separates the two regions and the theoretical activation energy for H_3^+ formation and its KER in the Coulomb explosion is marked with an arrow.

After roaming is initialised from the dication, it can either successfully abstract a proton if there is sufficient vibrational energy to enable the H_2–H^+ bond formation, but if not the system dissociates *via* pathway *X* to the $H_2/H^+/C_3H_3^+$ fragment pair. This is schematically shown in Fig. 7, where the geometrical structures are obtained from Oghbaie *et al.*[26] In this study the exact structure of the ring opened dication is not established, the structure has previously been thoroughly studied by Mayer *et al.*[38] The aforementioned dynamics suggest that a vibrational mode is of great importance to the roaming mechanism, in addition to the shallow static potential energy surface needed to retain the roaming particle. Of course, the first sign of the roaming motion involved a vibrational excitation in formaldehyde.[6] A lot of focus have previously been put on understanding the conditions for initiating the roaming mechanism, Stamm *et al.* provided three such conditions for several methyl halogens and pseudohalogens.[39] The cyclopropane dication, following the scheme described in Fig. 7 and the kinetic energy fulfills all the stated conditions. However, these conditions are based only on successful abstraction of the proton and formation of H_3^+ and not the channels that roam, but fail to abstract a fragment from the parent. A further study of how, in general, these interrupted roaming channels adhere to the conditions would contribute much to the field.

One might speculate that an associated vibrational mode within the parent molecule plays an even larger role than previously believed in the roaming dissociation mechanics. The role of not only providing the necessary energy to form the product, as shown in this study, but also to guide the neutral moiety on its roaming path. Further studies on the effects of the vibrational mode during the roaming motion might therefore illuminate the roaming mechanism further.

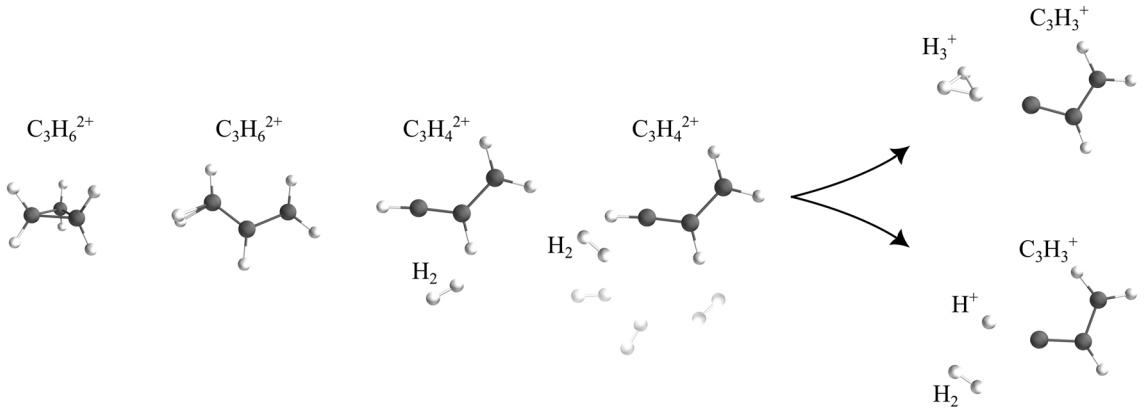

Fig. 7 A schematic of the formation process of H_3^+ including the roaming mechanism. The process starts with a dication (far left). The dication undergoes ring-opening into propene from which a neutral H_2 is emitted. The H_2 is captured on a shallow potential energy surface in which it roams around the dication. In the end the H_2 either abstracts a proton from the dication $C_3H_4^{2+}$ forming the H_3^+ ion or the roaming is interrupted and a C–H bond breaks, leading to the observed ions in coincident pair of $C_3H_3^+/H_3^+$ or $H_2/H^+/C_3H_3^+$, respectively.

This is suggested to be most easily accessed through pump–probe schemes with a probe in the IR regime to access the vibrational frequencies. Alternatively utilising the recent advances in attochemistry/femtochemistry to probe the ultrafast dynamics on the timescale of the vibration.

Conclusion

We have with momentum imaging shown that the formation pathway of the H_3^+ ion in the fragmentation of cyclopropane occurs *via* a roaming mechanism, specifically the roaming of a neutral H_2 moiety around the dication $C_3H_4^{2+}$. This is the first directly measured evidence that the roaming mechanism can also be accessed through inner-shell excitation and subsequent Auger–Meitner decay, although the product, H_3^+, has previously been detected after core ionisation. Furthermore, we show that, contrary to earlier studies, the neutral moiety shows significantly higher kinetic energy, which is suggested to be necessary to have enough energy to form the bond during the production of H_3^+. We also conclude that the stability of the dication around which the neutral moiety roams and the associated vibrational mode of the charged reactant are crucial for the roaming mechanism to occur.

Conflicts of interest

There are no conflicts to declare.

Data availability

Data for this article are available at Zenodo at https://doi.org/10.5281/zenodo.17867535.

Supplementary information: momentum analysis of alternative fragmentation pairs, determination of neutral product, total kinetic energy release calculation, and Fig. S1–S3. See DOI: https://doi.org/10.1039/d5cp04926a.

Acknowledgements

We are grateful to the staff of the FlexPES beamline at MAX IV in Lund, Sweden. We acknowledge the MAX IV Laboratory for beamtime on the FlexPES beamline under proposal 20220167. Research conducted at MAX IV, a Swedish national user facility, is supported by Vetenskapsrådet (Swedish Research Council, VR) under contract 2018-07152, Vinnova (Swedish Governmental Agency for Innovation Systems) under contract 2018-04969 and Formas under contract 2019-02496.

References

1 F. Gel'mukhanov and H. Ågren, *Phys. Rev. A*, 1996, **54**, 379.
2 O. Björneholm, M. Bässler, A. Ausmees, R. Feifel, H. Wang, C. Miron, M. N. Piancastelli, S. Svensson, S. L. Sorensen, F. Gel'mukhanov and H. Ågren, *Phys. Rev. Lett.*, 2000, **84**, 2826.
3 J. Laksman, E. P. Månsson, A. Sankari, D. Céolin, M. Gisselbrecht and S. L. Sorensen, *Phys. Chem. Chem. Phys.*, 2013, **15**, 19322–19329.
4 K. Ueda, A. De Fanis, N. Saito, M. Machida, K. Kubozuka, H. Chiba, Y. Muramatu, Y. Sato, A. Czasch, O. Jaguzki, R. Dörner, A. Cassimi, M. Kitajima, T. Furuta, H. Tanaka, S. Sorensen, K. Okada, S. Tanimoto, K. Ikejiri, Y. Tamenori, H. Ohashi and I. Koyano, *Chem. Phys.*, 2003, **289**, 135–147.
5 E. Kokkonen, K. Jänkälä, M. Patanen, W. Cao, M. Hrast, K. Bučar, M. Žitnik and M. Huttula, *J. Chem. Phys.*, 2018, **148**, 174301.
6 D. Townsend, S. A. Lahankar, S. K. Lee, S. D. Chambreau, A. G. Suits, X. Zhang, J. Rheinecker, L. B. Harding and J. M. Bowman, *Science*, 2004, **306**, 1158–1161.
7 P. L. Houston and S. H. Kable, *Proc. Natl. Acad. Sci. U. S. A.*, 2006, **103**, 16079–16082.
8 B. R. Heazlewood, M. J. T. Jordan, S. H. Kable, T. M. Selby, D. L. Osborn, B. C. Shepler, B. J. Braams and J. M. Bowman, *Proc. Natl. Acad. Sci. U. S. A.*, 2008, **105**, 12719–12724.

9 S. Maeda, K. Ohno and K. Morokuma, *J. Phys. Chem. Lett.*, 2010, **1**, 1841–1845.
10 M. P. Grubb, M. L. Warter, H. Xiao, S. Maeda, K. Morokuma and S. W. North, *Science*, 2012, **335**, 1075–1078.
11 T. Okino, Y. Furukawa, P. Liu, T. Ichikawa, R. Itakura, K. Hoshina, K. Yamanouchi and H. Nakano, *J. Phys. B: At., Mol. Opt. Phys.*, 2006, **39**, S515.
12 A. M. Mebel and A. D. Bandrauk, *J. Chem. Phys.*, 2008, **129**, 224311.
13 M. J. Bowman and A. G. Suits, *Phys. Today*, 2011, **64**, 33–37.
14 J. M. Bowman, *Mol. Phys.*, 2014, **112**, 2516–2528.
15 J. M. Bowman and P. L. Houston, *Chem. Soc. Rev.*, 2017, **46**, 7615–7624.
16 D. Mishra, A. C. LaForge, L. M. Gorman, S. Díaz-Tendero, F. Martín and N. Berrah, *Nat. Commun.*, 2024, **15**, 6656.
17 M. Nakamura, P.-Y. Tsai, T. Kasai, K.-C. Lin, F. Palazzetti, A. Lombardi and V. Aquilanti, *Faraday Discuss.*, 2015, **177**, 77–98.
18 A. Lombardi, F. Palazzetti, V. Aquilanti, H.-K. Li, P.-Y. Tsai, T. Kasai and K.-C. Lin, *J. Phys. Chem. A*, 2016, **120**, 5155–5162.
19 A. K. Rauta and B. Maiti, *Chem. Phys. Lett.*, 2016, **661**, 83–88.
20 D. Mishra, J. Reino-González, R. Obaid, A. C. LaForge, S. Díaz-Tendero, F. Martín and N. Berrah, *Phys. Chem. Chem. Phys.*, 2022, **24**, 433–443.
21 N. Ekanayake, T. Severt, M. Nairat, N. P. Weingartz, B. M. Farris, B. Kaderiya, P. Feizollah, B. Jochim, F. Ziaee, K. Borne, K. Raju, K. D. Carnes, D. Rolles, A. Rudenko, B. G. Levine, J. E. Jackson, I. Ben-Itzhak and M. Dantus, *Nat. Commun.*, 2018, **9**, 5186.
22 C. D. Foley, C. Xie, H. Guo and A. G. Suits, *Science*, 2021, **374**, 1122–1127.
23 T. Endo, S. P. Neville, V. Wanie, S. Beaulieu, C. Qu, J. Deschamps, P. Lassonde, B. E. Schmidt, H. Fujise, M. Fushitani, A. Hishikawa, P. L. Houston, J. M. Bowman, M. S. Schuurman, F. Légaré and H. Ibrahim, *Science*, 2020, **370**, 1072–1077.
24 N. Ekanayake, M. Nairat, B. Kaderiya, P. Feizollah, B. Jochim, T. Severt, B. Berry, K. R. Pandiri, K. D. Carnes, S. Pathak, D. Rolles, A. Rudenko, I. Ben-Itzhak, C. A. Mancuso, B. S. Fales, J. E. Jackson, B. G. Levine and M. Dantus, *Sci. Rep.*, 2017, **7**, 4703.
25 J. Tennyson, *Rep. Prog. Phys.*, 1995, **58**, 421.
26 S. Oghbaie, M. Gisselbrecht, E. P. Månsson, J. Laksman, C. Stråhlman, A. Sankari and S. L. Sorensen, *Phys. Chem. Chem. Phys.*, 2017, **19**, 19631–19639.
27 S. Kwon, S. Sandhu, M. Shaik, J. Stamm, J. Sandhu, R. Das, C. V. Hetherington, B. G. Levine and M. Dantus, *J. Phys. Chem. A*, 2023, **127**, 8633–8638.
28 A. Preobrajenski, A. Generalov, G. Öhrwall, M. Tchaplyguine, H. Tarawneh, S. Appelfeller, E. Frampton and N. Walsh, *J. Synchrotron Radiat.*, 2023, **30**, 831–840.
29 S. Ganguly, PhD thesis, Lund University, 2023.
30 D. Duflot, S. Zeggari and J.-P. Flament, *Chem. Phys.*, 2006, **327**, 518–528.
31 T. A. Field and J. H. Eland, *Chem. Phys. Lett.*, 1993, **211**, 436–442.
32 R. H. Dalitz, *Phys. Rev.*, 1954, **94**, 1046–1051.
33 J. Laksman, E. P. Månsson, C. Grunewald, A. Sankari, M. Gisselbrecht, D. Céolin and S. L. Sorensen, *J. Chem. Phys.*, 2012, **136**, 104303.
34 N. Neumann, D. Hant, L. P. H. Schmidt, J. Titze, T. Jahnke, A. Czasch, M. S. Schöffler, K. Kreidi, O. Jagutzki, H. Schmidt-Böcking and R. Dörner, *Phys. Rev. Lett.*, 2010, **104**, 103201.
35 S. Hsieh and J. H. D. Eland, *J. Phys. B: At., Mol. Opt. Phys.*, 1997, **30**, 4515.
36 T. Severt, J. Rajput, B. Berry, B. Jochim, P. Feizollah, B. Kaderiya, M. Zohrabi, F. Ziaee, K. R. P, D. Rolles, A. Rudenko, K. D. Carnes, B. D. Esry and I. Ben-Itzhak, *Phys. Rev. A*, 2024, **110**, 053104.
37 I. I. Mizus, O. L. Polyansky, L. K. McKemmish, J. Tennyson, A. Alijah and N. F. Zobov, *Mol. Phys.*, 2019, **117**, 1663–1672.
38 P. M. Mayer and L. Radom, *Chem. Phys. Lett.*, 1997, **280**, 244–250.
39 J. Stamm, S. S. Priyadarsini, S. Sandhu, A. Chakraborty, J. Shen, S. Kwon, J. Sandhu, C. Wicka, A. Mehmood, B. G. Levine, P. Piecuch and M. Dantus, *Nat. Commun.*, 2025, **16**, 410.